Crystallizations, Solid-State Phase Transformations and Dissolution Behavior Explained by Dispersive Kinetic Models Based on a Maxwell−Boltzmann Distribution of Activation Energies: Theory, Applications, and Practical Limitations

Peter J. Skrdla†

Merck & Company, Inc., RY818-B205, P.O. Box 2000, 126 East Lincoln Avenue, Rahway, New Jersey 07065, and 640 Maple Street, Westfield, New Jersey 07090

Received: May 14, 2009

The potential applications of dispersive kinetic models range from solid-state conversions to gas-phase chemical physics and to microbiology. Here, the derivation and application of two such models, for use in solid-state applications, is presented. The models are based on the concept of a Maxwell−Boltzmann distribution of activation energies. The ability of the models to fit/explain an assortment of asymmetric, sigmoidal conversion-versus-time transients presented in the recent literature, as well as to provide physicochemical interpretations of the kinetics via the two fit parameters, α and β, makes them a powerful tool for understanding nucleation/denucleation rate-limited processes that are involved in many phase transformations, dissolutions and crystallizations.

Introduction

A. Background and Goals. In the 1930s/1940s, Johnson and Mehl,[1] Avrami,[2−4] and Erofe'ev[5] published crystal physics descriptions of solid-state kinetics based on a nucleation-and-growth mechanism. The key outcome of their efforts was the popular "Avrami equation", also commonly referred to in the literature as the Johnson−Mehl−Avrami−Erofe'ev (JMAE) model, the Johnson−Mehl-Avrami−Erofe'ev−Kolgomorov (JMAEK) equation, the Avrami−Erofe'ev mechanism, and JMA model, as well as, cumulatively, the A1 (aka Prout−Tompkins[6,7]), A2, and A3 models. Written in integrated form, the Avrami equation is given by

$$[-\ln(x)]^n = kt \tag{1}$$

where x is the amount of "reactant phase" remaining in the system (hence, the difference, $1 - x$, represents the fractional conversion to the "product phase") at time, t, k is the rate constant of the process and $n = 1, {}^1/_2, {}^1/_3$ or, depending on whether the (random, homogeneous) nucleation occurs in one, two, or three dimensions, respectively.

Other commonly employed (isothermal) models for treating the title phenomena in which nuclei are important, such as the Šesták−Berggren model and the extended/generalized Prout−Tompkins equation (of Burnham and Braun[8]), will not be discussed here because they were described in the author's previous papers (see references section) and also reviewed in recent articles.[9,10] To date, the Avrami equation appears to be the simplest model with the broadest application (hence, arguably the current "gold standard"), but it is not without limitations. For example, in eq 1 x cannot be zero or the left-hand side term is undefined. Additionally, because the values of n listed above often do not support good curve fits to empirical data, n is frequently afforded the flexibility to take on any empirically determined value. As the parameter has no units, its physical interpretation is often ambiguous, which limits its overall utility.

It is easy to recast eq 1 in the form of a "stretched exponential", as shown below:

$$\ln(x) = -k_0 t^{1/n} \tag{2}$$

where the rate constant, k_0, was given a subscript to highlight the fact that it is not mathematically equivalent to k in eq 1. Stretched exponentials have gained recent acceptance in a wide variety of applications, including studies of tumor growth rates (using so-called "fractal kinetics")[11] and investigations into the origin of allometric scaling laws in biology (as supported by the novel concept of "quantum metabolism").[12] Plonka[13−15] has employed the concept of fractal conversion time to show that the Avrami equation is an outcome of the dispersive (aka "distributed") kinetics approach. Dispersive kinetics are observed in chemical reactions or phase transformations in which the rate of internal rearrangements (e.g., molecular relaxation) responsible for producing continuous "system renewals", is similar to, or slower than, the rate of the overall conversion. Since dispersive kinetics can occur in all phases of matter (as well as in biological systems, as mentioned above) and over vastly different time scales, the study of these phenomena is core to many areas of present-day chemical/biochemical/materials research. The use of fractals is only one possible approach for describing dispersive kinetics.

As already stated, the importance of dispersive kinetics reaches far beyond solid-state systems, which are the focus of the present work. For example, it has recently been discussed that the activation energy barrier crossing in the enzyme, purine nucleoside phosphorylase (PNP), occurs via coordinated molecular dynamic motions occurring on the femtosecond time scale. In their work, Saen-oon et al.[16] described how the activation entropy of the transition-state (TS) species is linked to the dynamics of the protein, analogous to the present author's proposed link between the activation entropy and molecular motion (kinetic energy) in solid-state dispersive kinetics.[17]

† E-mail: peter_skrdla@merck.com, skrdla@earthlink.net.

10.1021/jp904505w CCC: $40.75
Published on Web 07/24/2009

Essentially, the "TS ensemble" has a distribution of momenta along various reaction trajectories, which is thought to create a "stochastic separatrix" (analogous to the author's "distribution of activation energies", discussed more later) between the reactant and product states. The inherent thermal motion in the enzyme changes the shape of the activation energy barrier, thus facilitating the catalyzed reaction via so-called "promoting vibrations" of the TS complex. It is pointed out here that the femtosecond sigmoidal transients observed in that system, on the atomic level (i.e., for a single enzyme/substrate), are not unlike those presented in this work (which are observed on a much longer time scale and relate to a large ensemble of molecules), with the exception of the oscillatory feature observed at midconversion in the former system that is attributed to the finite lifetime of the TS complex (note that this feature is not present in the transients of lactate dehydrogenase, which is thought to proceed via a more concerted reaction). Since molecular vibrations are quantized, the activation energy might therefore also be quantized, to some extent; this observation has implications on the current author's use of the Maxwell−Boltzmann (M−B) distribution. It is possible that in enzymatic systems, as in dispersive solid-state kinetics, the activation energy barrier has both a thermodynamic component, described by the enthalpy of activation, and a dynamic component, related via the activation entropy. Particularly for low-barrier enzymatic reactions, dynamical effects can become important in accurately describing the overall kinetics. It is noted here that one of the author's dispersive kinetic models, presented later, has been previously applied to gas-phase femtosecond reactions that have a short-lived transition state (TS), i.e., those that do not exhibit internal vibrational redistribution (IVR).[18] On the other hand, in cases where IVR is important for energy dissipation (relaxation), the TS of simple reactions often exhibits a periodic/oscillatory rate coefficient[19] that is termed "vibrational coherence" when observed experimentally. The similarities between dispersive kinetics on the femtosecond time scale and those on second/minute time scales will be discussed more in future works.

Dispersive kinetics is sometimes also called "stochastic kinetics" as it pertains to studies of the on/off function of so-called "molecular switches" or biological ion channels, for example, whereby the results (e.g., the time intervals separating the "on"/"open" and "off"/"closed" states) are interpreted with the aid of (e.g., Brownian motion) statistics. Plonka showed[13,14] that dispersive kinetics is responsible for creating a *time dependence* in both the rate constant (thus, more appropriately called the "rate coefficient") and the activation energy. However, as time-dependent rate coefficients and activation energies appear to go against classical kinetics (e.g., the Arrhenius equation), such findings might be easily dismissed by workers who are unfamiliar with the field. One of the goals of this work is to highlight some of the underlying concepts in dispersive kinetics.

In lieu of using the Kohlrausch−Williams−Watts (KWW) relaxation function as the basis for developing a general treatment of dispersive kinetics based on the concept of fractal conversion time (whereby the KWW function is used to define the time-dependent rate coefficient),[13,14] it is possible to develop a treatment that is based on the a priori assumption of an activation energy distribution having a specific functional form (e.g., the M−B) which, in turn, relates a specific functional form (e.g., a Gaussian) of the time-dependent rate coefficient. Additional discussion of the latter topic seems necessary due to the fact that some recent feedback[20] has indicated that this approach might be "evidently sophisticated (mathematically)" and produces a "possibly more complicated theory" than other solid-state kinetic modeling approaches. For that reason, the present work will summarize, completely and in one location, in the simplest possible mathematical terms, the development of two (related) dispersive kinetic models that the author has used in multiple applications to-date, which are based on the assumption of a M-B distribution of activation energies. Both models have an easy-to-use, closed-form analytical solution with only two, physically relevant fit parameters.

It is especially important to clarify the mathematical treatment in this paper to ensure the accuracy and consistency of the equations that were developed and published previously in various journals, as well as to highlight and to discuss any approximations that were used in their derivation. Additionally, to address any concerns that might exist regarding the "experimental background" of the solid-state systems investigated to date,[20] the two models will be applied here to an array of recently published (by workers other than the author) kinetic data to demonstrate their broad applicability as well as to point out any pitfalls (problems) that one might potentially encounter during the modeling. In accomplishing that goal, it is thought that the use of dispersive kinetic models might gain wider acceptance.

B. Theory, Part 1: Development of Dispersive Kinetic Models To Fit Acceleratory and Decelerator Conversion−Time ($x-t$) Transients Based on a Maxwell−Boltzmann Distribution of Activation Energies. Dispersive kinetics are frequently characterized by sigmoidal $x-t$ transients. Additionally, they are often asymmetrical about the inflection point, resulting in curves that are either "acceleratory" (whereby the reaction speeds up as $x \rightarrow 0$, postinduction period) or "decelerator" (whereby the conversion rate slows down as $x \rightarrow 0$, postinduction period) in appearance. Acceleratory transients are typically synonymous with heterogeneous systems, while decelerator ones often pertain to homogeneous conversions. Examples of heterogeneous conversions include (some) nucleation-and-growth rate-limited polymorphic phase transformations conducted under slurry conditions. Examples of homogeneous conversions include the (denucleation rate-limited) thermal decomposition of many types of crystals.

The distinct asymmetry in the empirical data of dispersive conversions is often poorly handled by standard models like the Prout−Tompkins (autocatalytic) model and Gompertz model, which lack "dimensionality" (n). An interesting consideration provided by the Gompertz model, which, since its first appearance in the literature in 1825 has mostly appeared in biological applications, is that it assumes a first-order mechanism having a time-dependent rate coefficient;[21] this fundamental assumption is entirely consistent with that made in the development of more recent models for treating dispersive kinetics, as mentioned above.

Specifically, the rate coefficient, k, has the following functional form in the Gompertz model:

$$k = \alpha e^{\beta t} \tag{3}$$

where α and β are empirical constants (each with units of inverse time). Substituting eq 3 into the integrated expression for a first order mechanism for a reaction with a time-dependent rate coefficient, specifically:

$$x = e^{-\int_0^t k dt} \tag{4}$$

one obtains the Gompertz model, shown below:

$$x = e^{(-\alpha/\beta)[e^{\beta t}-1]} \quad (5)$$

The type of activation energy distribution that is responsible for producing the time dependence of the rate coefficient in eq 3 has not been previously specified, to the author's knowledge. Perhaps, for that reason, eq 5 has remained most popular in biological applications.

Focusing now on the M−B distribution, it is noted that the distribution was originally developed to describe the distribution of speeds in an ideal gas at thermodynamic equilibrium. However, the functional form of this distribution might also be useful in relating the distribution of kinetic energies (i.e., the dynamics) of either the reactant population (in a deceleratory conversion) or the "activated" species (in a acceleratory conversion) in solid-state applications.[16,18,22] That is because the M−B distribution treats particles as distinguishable units and it is known that atoms/molecules comprising either solids or critical nuclei (as they relate to the rate-determining step, rds, of a conversion) can be expected to experience different energies due to their different spatial locations. In the solid-state dispersive kinetics of insulating materials, the distribution of activation energies might be linked mainly either to the thermal phonons in the *reactant solid* (for deceleratory conversions) or to the thermal phonons in the *activated state*, "AS", i.e., the so-called critical nuclei (for acceleratory conversions). That is because these energy states can be thermally activated at moderate temperatures and, via normal fluctuations, they produce a mathematically smooth distribution on the macroscopic level (note that, previously, the author has described those energies as "the monomer kinetic energies"). The potential role of plasmons in the formation of metallic nanoparticles is also of interest here. Phonon/plasmon modes in solids are analogous to molecular vibrations that are known to cause dispersion in femtosecond kinetics (as well as coherence/periodicity, for longer-lived TS species[18,23]) and they might be responsible for producing the attractive/repulsive forces needed for nucleation/denucleation (and hence defining the underlying system dynamics in the rds; more discussion on that point will come in future works). The other types of particle energy distributions commonly encountered in statistical mechanics, namely the Bose−Einstein (which pertains to *indistinguishable* bosons, like phonons and plasmons) and Fermi−Dirac distributions, revert to the M−B distribution when the ensemble is at high temperature and/or at low concentration. Thus, for the purposes of this work, the use of the M−B distribution seems appropriate.

The M−B distribution can be expressed in terms of the monomer kinetic energies, ε_K, as follows:

$$\left(\frac{1}{N}\right)\left(\frac{dN}{d\varepsilon_K}\right) = \left(\frac{2}{\sqrt{\pi}}\right)\left(\frac{1}{k_B T}\right)^{3/2}(\varepsilon_K)^{1/2}(e^{-\varepsilon_K/k_B T}) \quad (6)$$

where N is the number of molecules (monomers) in the ensemble, k_B is the Boltzmann constant, and T is the absolute temperature. Since the activation energy distribution that is sought will be the sum of potential ($\Delta H^{\ddagger}$, fixed) and dynamic ($\Delta S^{\ddagger}$, t-dependent) contributions, as alluded to in the Introduction, the shape of the kinetic energy distribution, $D(\varepsilon_K)$, in eq 6 should mirror that of the activation energy distribution, $D(\varepsilon_a)$, where ε_a represents the individual monomer activation energy barrier. The reason for that is evident from transition state theory (TST) and collision theory (CT); the "energy offset" (a constant) from the zero-point energy to the AS energy relates the enthalpic contribution, while the entropic contribution to $D(\varepsilon_a)$ is defined by the distribution of thermally activated (phonon/plasmon) states in either the reactant or AS species.

In line with time-dependent Marcus theory (TDMT),[18,22,24] the overall shape of $D(\varepsilon_a)$ is dependent on both the time-independent activation energy potential, E_a (or $\Delta H^{\ddagger}$, as described above), and the time-dependent reorganization energy, $\lambda(t)$ (or $\Delta S^{\ddagger}$), pertaining to the rds of the conversion. Whether $\lambda(t)$ relates predominantly to the reactant solid (for a homogeneous conversion/deceleratory trend) or to the AS (acceleratory trend) affects whether the time-dependent activation energy of the conversion increases or decreases (respectively) with conversion time. The two types of activation energy distributions that can be applied to acceleratory and deceleratory dispersive processes have been described in detail elsewhere.[16,18,22] Briefly, the energy-level diagram for a dispersive process is not a two-state one, as per classical Arrhenius kinetics, but rather a multistate one, in which either the AS or the reactant species is largely responsible for producing the multitude of states that ultimately makes up $D(\varepsilon_a)$. The latter case is somewhat analogous to the phenomenon of Raman scattering, whereby the AS is akin to a higher energy, "virtual state" and the energy level difference between adjacent reactant state levels is on the order of $\leq k_B T$, for many systems. The acceleratory case can be thought of as complementary to the case of deceleratory kinetics.

Solving the Arrhenius definition of a rate constant, specifically:

$$k = Ae^{-\Delta\varepsilon_a/k_B T} \quad (7)$$

(where A is the Arrhenius constant or "frequency factor", with units of s^{-1}) for ε_a and substituting the result into eq 6 (for ε_K), then rearranging the subsequent expression (which describes $D(k)$, the rate coefficient distribution), one obtains the following nonlinear differential equation, expressed in terms of k:

$$k = Ae^{-\pi(A/2N)^2(dN/dk)^2} \quad (8)$$

Given that A, N, and π are constants, eq 8 takes the following general form:

$$k = Ae^{B(dN/dk)^2} \quad (9)$$

where $B = -\pi A^2/4N$,[2] with units of s^{-2}. Using a graphical representation of $D(k)$, not shown, it is possible to approximate dN/dk as being linear as $dk \rightarrow 0$, for any value of k.[26] As the value of dN/dk in $D(k)$ is dependent on that of k, and since each k has units of inverse time, dN/dk is inversely related to the individual monomer conversion time. The individual conversion times (and the fraction of monomers undergoing conversion with each given rate constant), in turn, dictate the overall (i.e., observed) conversion time, t. Thus, a reasonable approximation for the differential might be provided by

$$\frac{dN}{dk} = \gamma t \quad (10)$$

where γ is a unitless constant. Using this approximation in eq 9, one obtains the following relation describing the time-dependence of the rate coefficient for dispersive kinetic processes that have an "M−B-like" distribution of activation energies:

$$k = \alpha e^{\beta t^2} \tag{11}$$

where the new constant, β, has units of s^{-2} (note that $\beta = B\gamma^2$; also, A has been generalized to the new constant, α, to allow for reaction dimensionalities other than zero to be considered as well as to support the classical/"potential component" activation energy, ε_a^0 ($\sim\Delta H^{\ddagger}$), to be incorporated into it; see eq 19). The parameter, β, in eq 11 can be either positive or negative, depending on whether the conversion is acceleratory or deceleratory, respectively. Note that the Gaussian form of the expression for k in eq 11 is in sharp contrast to the empirical expression put forth in eq 3 that ultimately yields the Gompertz model. Substituting eq 10 and eq 11 in eq 9, it is possible to mathematically verify the result. An important point to highlight here is the fact that the functional form of k in eq 11 is reminiscent of that of the Debye−Waller factor that describes thermal dissipation in solids; this point serves both to further verify the physicochemical validity of the equation and to lend additional support to the initial selection of the M−B distribution to describe activation energy distributions in solid-state dispersive kinetics. Finally, it is noted here that TDMT also supports the functional form of eq 11 (for short-lived TS species in femtosecond dynamical studies[19,27]).

It is highlighted here that in eq 11, if no effects from a distribution of rate constants are observed in the conversion kinetics (i.e., the overall rate is not influenced by continuously changing/evolving molecular environments in the system under investigation) and hence no t-dependence of the rate coefficient is observed, $\beta = 0$ and, consequently, $k = \alpha$, which is a constant, consistent with the classical Arrhenius description of the rate constant. Using $k = \alpha$ in the ensuing derivations would simply result in a (nondispersive) first-order kinetic model.

As per the derivation of the Gompertz equation, it is possible to use the expression for k in eq 11, substituted into eq 4 (note that the majority of known chemical reactions obey first-order kinetics, so it is a good initial choice) and subsequently integrated, to obtain a first-order dispersive kinetic model for acceleratory, sigmoidal $x-t$ trends. However, if integrated directly, the result necessitates use of the (imaginary) error function.[25] To obtain a closed-form analytical solution, one must use an approximation for k in eq 11. It has been shown[19] that

$$k = -\left[\left(\frac{\alpha}{t^2}\right)(e^{\beta t^2} - 1) + 2\alpha\beta e^{\beta t^2}\right] \tag{12}$$

is a good approximation. Using eq 12 in eq 4, as stated above, the resulting model is given by

$$x = e^{(-\alpha/t)(e^{\beta t^2}-1)} \tag{13}$$

Note the similarity in functional form of this equation to the Gomerptz model. As eq 13 describes the loss of starting material as a function of time, to obtain the complementary model for the growth of the product fraction, p (note: $p = 1 - x$), one simply writes

$$p = 1 - e^{(-\alpha/t)(e^{\beta t^2}-1)} \tag{14}$$

In both eq 13 and eq 14, β can be expected to be positive (as written) when its value is extracted from curve fits of acceleratory data.

Equation 4 can be generalized to allow consideration of dimensionalities other than zero by incorporating a t^n term in front of the integral, as shown here:

$$x = e^{-(t^n)(\lim_{a\to 0}\int_a^t k\,dt)} \tag{15}$$

In the author's experience, the case where $n = 2$ is most effective in describing the majority of deceleratory $x-t$ transients, likely due to the fact that critical nuclei surfaces, whose energies are thought to be most influential in determining the rate of conversion in nucleation/denulceation rate-limited (i.e., dispersive) conversions, can be approximated as being two-dimensional (2D). The limit is present in eq 15 because k is undefined at $t = 0$ in the present approximations to eq 11 (i.e., eq 12 and also in eq 16, provided below). Using eq 15 (with $n = 2$) together with eq 16 (the approximation for k where β is explicitly shown to be negative)

$$k = \left[\left(\frac{\alpha}{t^2}\right)(e^{-\beta t^2} - 1) + 2\alpha\beta e^{-\beta t^2}\right] \tag{16}$$

yields the following first-order, deceleratory dispersive model:

$$x = e^{(\alpha t)(e^{-\beta t^2}-1)} \tag{17}$$

As per the acceleratory (1D, i.e., $n = 0$) variant of this equation (eq 13), the dependence of the product fraction on the conversion time is given by

$$p = 1 - \{e^{(\alpha t)(e^{-\beta t^2}-1)}\} \tag{18}$$

C. Theory, Part 2: Physicochemical Relevance of the Fit Parameters in Kinetic Modeling Applications. Equipped with the above models (eq 13/eq 14 and eq 17/eq 18), one can attempt curve fits of even the most challenging dispersive kinetic data, as will be discussed in the next section. However, to extract meaning from the empirical trends, it is necessary to have physical interpretations for the constants, α and β. These can be provided most readily using the Gaussian form of the time-dependent expression for k, given by eq 11, by applying both TST and CT outcomes. It has been shown that the two rate parameters have the following physical interpretations (note that eq 19 is written for the general case, with arbitrary n):[16,22]

$$\alpha = A^{n-1}e^2e^{-E_a^0/RT} = A^{n-1}e^{-\Delta H^{\ddagger}/RT} \tag{19}$$

where A is an "Arrhenius-like" factor with the entropic component of the molar Gibbs energy of activation, $\Delta G^{\ddagger}$ (see below), removed due to the fact that it is time-dependent, E_a^0 is the (t-independent) component of the overall activation energy, and R is the gas constant, and

$$\beta = \frac{\Delta S^{\ddagger}}{Rt^2} \tag{20}$$

where $\Delta S^{\ddagger}$ is the activation entropy of the conversion, which is both time- and, naturally, temperature-dependent. Equation 20 is interesting in its similarity to $E = mc^2$ (itself, an approximation). Note that from eq 19 onward, molar quantities are used

instead of molecular ones; hence, R appears in place of k_B in these equations and the physical parameters are assigned capital letters instead of lower case ones. It should be pointed out that eq 20 yields physically meaningful results only for values of t for which $0 \leq x < 1$, as β is undefined at $t = 0$ and the conversion is complete when $x = 0$ (this observation might be related to the Gibbs Paradox, stemming from the use of the M−B distribution).

Utilizing TST, one can write

$$E_a = E_a^0 - RT\beta t^2 \quad (21)$$

and

$$\Delta G^{\ddagger} = E_a^0 - 2RT - T\Delta S^{\ddagger} = \Delta H^{\ddagger} - T\Delta S^{\ddagger} \quad (22)$$

Substituting eq 19 and eq 20 into eq 11, making use of eq 21 and eq 22, yields the following results:

$$k = A^{n-1}e^2 e^{-E_a^0/RT} e^{\Delta S^{\ddagger}/R} = A^{n-1} e^{-\Delta H^{\ddagger}/RT} e^{\Delta S^{\ddagger}/R} = A^{n-1} e^{-\Delta G^{\ddagger}/RT} \quad (23)$$

which are entirely consistent with Eyring's definition of a rate constant, with the exception that, in dispersive kinetics, the rate coefficient has a t-dependent activation energy (or Gibbs energy of activation), which, ultimately, originates from the t dependence of $\Delta S^{\ddagger}$. This time dependence is a manifestation of the M−B energy distribution used at the outset of the derivation of the dispersive kinetic models, as described in the previous section, and it is to be expected from the dispersive kinetics literature, e.g., refs 13−15.

D. On the Physical Rigor of the Approach. The equations presented herein do not provide a statistical mechanical foundation for dispersive kinetics in terms of partition functions, and consequently, they do not explain nucleation/denucleation in terms of time- and temperature-dependent potentials of mean force. That is standard procedure in molecular dynamics (MD) modeling. However, the apparent "lack of rigor" of the present approach is no more prevalent, in the author's opinion, than in MD-type simulations in which the "invented" potential function is applied to a statistical ensemble that is often far too small to truly observe dispersive behavior.[27] Perhaps, as computational power increases in the future, as does the fundamental knowledge of the interaction potentials relevant to nucleation/denucleation (possibly, with the aid of the models described in this paper, or similar ones), MD simulations will provide the best description of the kinetic processes studied in this work. However, at present, the frequently huge discrepancy between predicted and observed nucleation rates observed from various molecular simulations in the recent literature supports the idea that a different approach might be needed to model such behavior, at least for the interim.

Results and Discussion

While the dispersive kinetic models, eq 13/eq 14 and eq 17/eq 18, have been applied previously to various reactions and phase transformations involving the solid-state (including polymorphic, e.g., ref 26, and solvate/anhydrate[27] interconversions, crystallizations[28] and drug dissolution[29]), in this paper their application to an array of quite different data sets, found in the recent literature, is described. The main purpose of this effort is to demonstrate the validity and robustness of these (isothermal) models with respect to a variety of systems. A secondary objective is to point out any limitations, pitfalls, or otherwise interesting findings/results that one might encounter when using them.

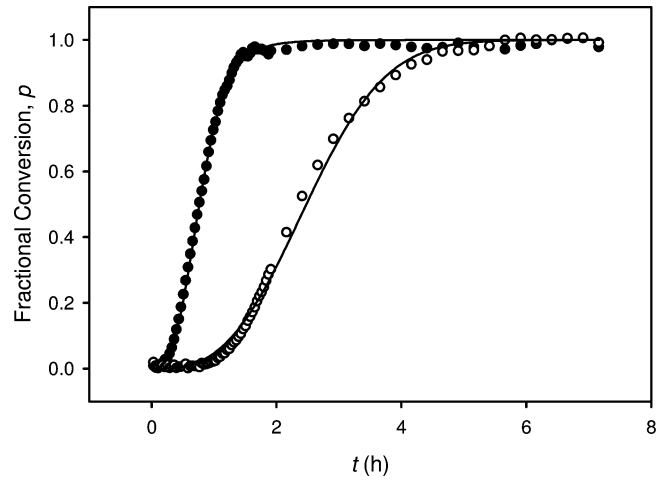

Figure 1. Fractional composition vs time plots constructed from Raman spectra for the slurry conversion of MK-A hemihydrate to form C, at 15 °C (○) and 25 °C (●). The values of the fit parameters extracted using eq 18 are as follows: $R^2 = 0.9974$, $\alpha = 2.14$ h^{-1}, $-\beta = 0.023$ h^{-2} (○); $R^2 = 0.9988$, $\alpha = 2.24$ h^{-1}, $-\beta = 0.89$ h^{-2} (●).

A. Solvent-Mediated Phase Transformation of "MK-A": An Example of a Deceleratory $x-t$ Transient. The first case studied was the phase transformation of the pharmaceutical compound, "MK-A", from the hemihydrate form to the crystalline Form C.[30] From Figure 1 it is clear that the formation of form C product is faster at 25 °C than at 15 °C, for this slurry transformation performed in dry isopropyl acetate. That finding suggests that the conversion is not nucleation rate-limited (in the product phase), as such a conversion would (1) exhibit faster kinetics at lower temperatures (that favor nucleation, due to the larger thermodynamic driving force provided by increasing the supersaturation) and (2) exhibit acceleratory sigmoidal kinetic trends,[26] not deceleratory ones. Rather, this heterogeneous conversion is more consistent with a denucleation rate-limited mechanism, meaning that the dispersive kinetics observed using in situ Raman spectroscopy of the solid phases is attributable to the dissolution[29] of the reactant phase, i.e., the hemihydrate.

Using eq 21 and the values of β provided in the figure caption (note that β is negative for deceleratory processes, as shown explicitly in the model, eq 18), it is possible to determine the time-dependent increase in the activation energy barrier for the conversion, at each of the two temperatures. Starting with a crude plot of the temperature dependence of α (i.e., an Arrhenius-type plot;[26] not shown here due to the fact that there are only two points in it), one can extract values for both A and E_a^0 (recall that $n = 2$ in eq 18). From the (expectedly) linear fit, which has a vertical intercept of −6.07 and a slope of −392.6 K, the following estimates were obtained: $A = 3.1 \times 10^{-4}$ s^{-1} and $E_a^0 = 3.3$ kJ/mol. Thus, at 25 °C (using $\beta = -0.89$ h^{-2}) E_a for the conversion increases by 2.2 kJ/mol after 1 h. This increase in the activation energy causes the rate deceleration observed in the curves in Figure 1, as described in Part B of the Introduction. However, as both A and E_a^0 are considerably lower than expected, it is likely that the conversion is an equilibrium process and not a "unidirectional", first-order one as assumed in the derivation of the model. Assuming that the dissolution of the reactant phase is an equilibrium processes implies that the *apparent* values of A, E_a^0, and E_a obtained

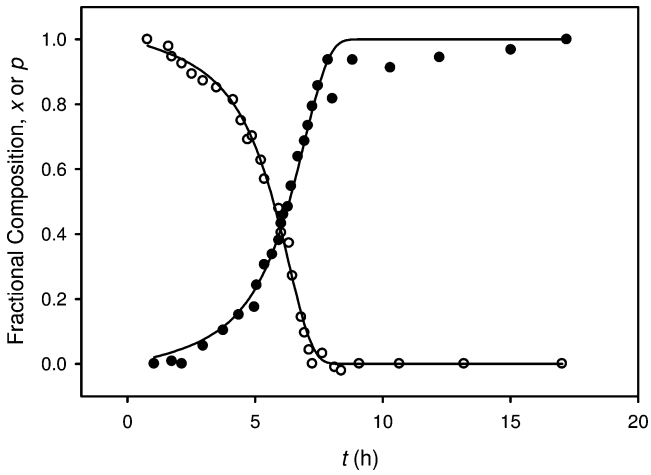

Figure 2. Fractional composition vs time plots constructed from Raman spectra for the conversion of the α form of L-glutamic acid to the β form, at 45 °C. Both the "reactant" (○) and "product" (●) kinetic trends are shown. The values of the fit parameters extracted using eq 13/eq 14 are as follows: $R^2 = 0.9957$, $\alpha = 0.301$ h, $\beta = 0.081$ h^{-2} (○); $R^2 = 0.9848$, $\alpha = 0.261$ h, $\beta = 0.072$ h^{-2} (●).

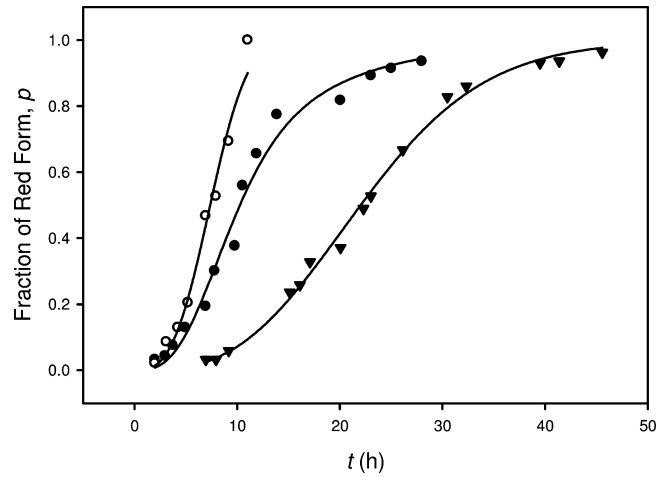

Figure 3. Fractional conversion vs time plots constructed from XRPD data for the conversion of the dark red form to the red form of the ROY derivative at 85 °C and 0% RH. The size of the crystals increases from left to right. The fit parameters extracted using eq 18 are as follows: $R^2 = 0.9796$, $\alpha = 6.93$ h^{-1}, $-\beta = 2.5 \times 10^{-4}$ h^{-2} (○); $R^2 = 0.9851$, $\alpha = 0.103$ h^{-1}, $-\beta = 1.0 \times 10^{-2}$ h^{-2} (●); $R^2 = 0.9956$, $\alpha = 0.106$ h^{-1}, $-\beta = 7.3 \times 10^{-4}$ h^{-2} (▼).

experimentally are, in fact, values of A_1/A_{-1}, ΔE_a^0 and ΔE_a, respectively (for the forward and reverse processes). That is because for the treatment of a reversible process, k must be replaced by the ratio, k_1/k_{-1}, in the derivation; doing so ultimately converts the kinetic quantities described in the previous section to either the corresponding "difference" or "ratio" terms. That is a key finding (and potential pitfall) from this example.

B. Solvent-Mediated Phase Transformation of L-Glutamic Acid: An Example of an Acceleratory $x-t$ Transient. The second example investigated involved another polymorphic phase transformation: the solvent-mediated conversion of the α form of L-glutamic acid to the β form (which was also monitored in situ via online Raman spectroscopy).[31] Figure 2 shows that a simpler approach for modeling the kinetics of this conversion, than that taken by the original authors, might be found in the use of the *acceleratory* dispersive kinetic model presented in this paper, eq 13/eq 14. As per the author's earlier works, the curvature of these sigmoids suggests that the phase transformation is product (β form) nucleation rate-limited, in sharp contrast to the previous example. The fit qualities are not as good as in the MK-A example, likely due to the poorer quality of the data (and not a limitation of the model) mainly because of the big difference between the R^2 values for the two curves (which should, ideally, be mirror images of each other). Unfortunately, as the data shown in Figure 2 pertains only to a single temperature, it is not possible to estimate the physical quantities as per the MK-A example.

Comparing the plots in Figure 2 to those in Figure 10 of the original work,[31] it can be seen that in the latter graphic the fractional composition of the α form actually increases during the initial stages of the conversion. These points were intentionally omitted in the present work due to the fact that they can be attributed to the dissolution of the α form (in trying to reach equilibrium solubility) at the outset of the experiment and they do not appear to impact the subsequent conversion kinetics. As one cannot expect to generate any of the β form until there is a significant quantity of the α form in solution (because supersaturation is needed to nucleate the β form), eq 20, which inherently contains a limit as $t \rightarrow 0$ (see Introduction), seems to make real sense in this case. That point, coupled with the observation that polymorphic phase transformations can be acceleratory as well as decelerating, is the key observation from this example.

C. Solid-State Phase Transformation of a ROY Derivative: The Effect of Particle Size on Conversion Rate. The third example came from Li et al.;[32] it deals with the kinetics of the solid-state phase transformations of the compound, 5-methyl-2-[(4-methyl-2-nitrophenyl)amino]-3-thiophenecarbonitrile, which is a "ROY" derivative. As shown in Figure 3, the dark red form of this compound turns into the red form with different conversion rates, depending on the size of the crystals of the starting form: the coarser the crystals, the faster the conversion rate and vice versa. This observation appears counter to that of the current author's previous work,[26] where it was discussed that smaller crystals, having higher surface energies, should convert more readily than large crystals despite having a longer induction period. However, Li et al.[32] concluded that the transformation rate in the present system was not crystal size-related but rather dominated by the crystal defect content (defects are well-known secondary nucleation sites). The *deceleratory* model, eq 18, was found to fit the empirical trends in Figure 3 reasonably well despite the notable paucity in the data points (obtained using offline X-ray powder diffraction, XRPD, monitoring). The deceleratory nature of the curve shapes are more consistent with a denucleation mechanism for the disintegration of the dark red crystals (as per the various crystal decomposition reactions that the present author has investigated), than a nucleation-based one (for the formation of the red phase). Thus, it can be concluded that defect sites can be promoting in denucleation-driven events as well as in nucleation-based phenomena. Additionally, this data set serves to demonstrate the utility of online monitoring techniques, as compared to offline ones, for monitoring solid-state conversions in that it clearly shows that (off-line sampling issues aside) more points are better, provided that the data is to be used in kinetic modeling (note that the original authors selected the 3D Avrami "random nucleation-and-growth" model for that purpose,[32] with fits seemingly comparable to those in the present Figure 3). Those are the two main findings stemming from this example.

D. Crystallization Rates of a Thiazole Derivative: Effect of Antisolvent Addition. In the fourth example, Kitamura and Hironaka[33] studied the antisolvent addition effects on the

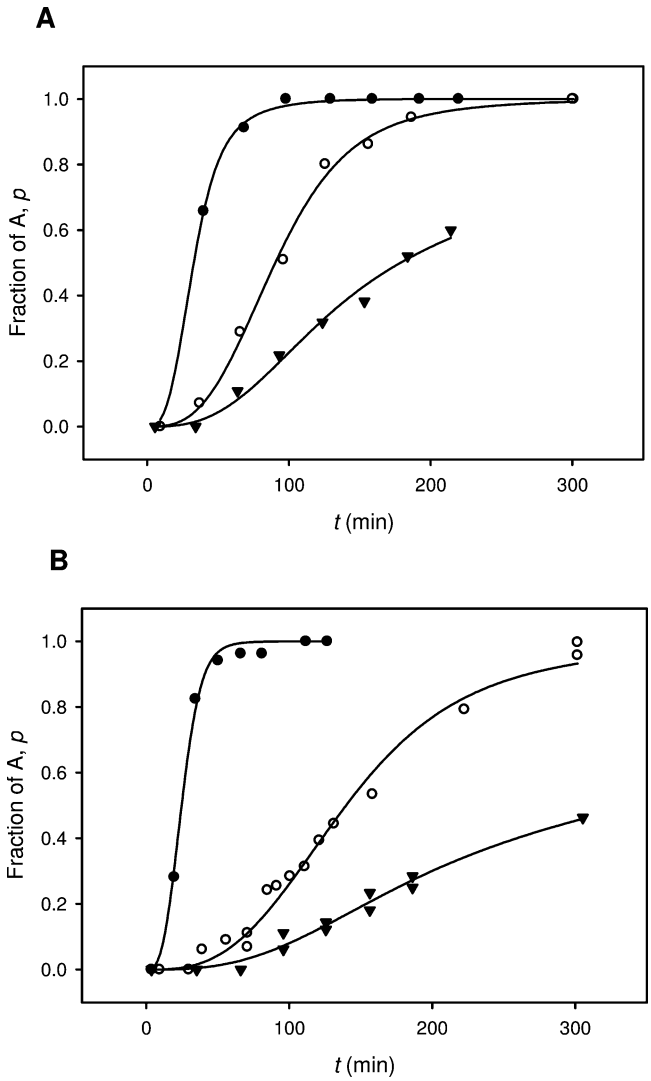

Figure 4. Fractional conversion vs time plots for the conversion of one crystalline form, BH, to the other, A, at 333 K (60 °C). (A) The initial BH concentration is 0.055 M; the water addition rates are as follows: 1.4 (●); 2.0 (○); 2.8 mL/min (▼). The fit parameters extracted using eq 18 are as follows: $R^2 = 0.9987$, $\alpha = 3.98 \times 10^{-2}$ min^{-1}, $-\beta = 7.1 \times 10^{-4}$ min^{-2} (●); $R^2 = 0.9959$, $\alpha = 0.016$ min^{-1}, $-\beta = 8.0 \times 10^{-5}$ min^{-2} (○); $R^2 = 0.9882$, $\alpha = 4.04 \times 10^{-3}$ min^{-1}, $-\beta = 1.0 \times 10^{-4}$ min^{-2} (▼) (B) The initial BH concentration is 0.079 M; the water addition rates are as follows: 1.4 (●); 2.0 (○); 2.8 mL/min (▼). The fit parameters extracted using eq 18 are as follows: $R^2 = 0.9955$, $\alpha = 8.32 \times 10^{-2}$ min^{-1}, $-\beta = 6.7 \times 10^{-4}$ min^{-2} (●); $R^2 = 0.9862$, $\alpha = 9.2 \times 10^{-3}$ min^{-1}, $-\beta = 4.0 \times 10^{-5}$ min^{-2} (○); $R^2 = 0.9775$, $\alpha = 2.03 \times 10^{-3}$ min^{-1}, $-\beta = 5.3 \times 10^{-5}$ min^{-2} (▼).

crystallization rates of different forms of a thiazole derivative. Figure 4A shows the effect of the water addition rate on the transformation kinetics of the "BH" form (a hydrate) to give the product crystal form, "A", where the initial concentration of BH was 0.055 M. Figure 4B shows the results of the same experiment, but with the initial BH concentration of 0.079 M. In both plots, the faster the antisolvent (water) addition rate, the slower the rate of the transformation. At the same time, the higher the starting concentration, the faster the turnover that was observed. While the latter is an expected result (from the Arrhenius equation), the original authors hypothesized that there must have been A present in the BH starting material to act as seed in the transformation, to explain the former observation (the amount of A seed produced was thought to increase with decreasing antisolvent addition rate).[33]

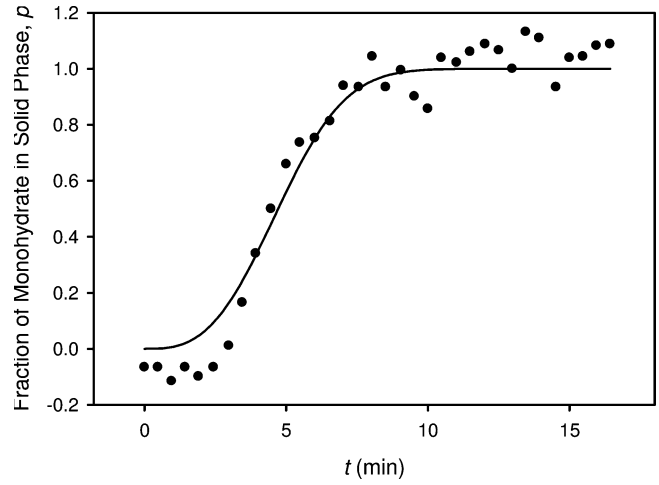

Figure 5. Fractional conversion vs time plot for the transformation of TP anhydrate to TP monohydrate. The fit parameters extracted using eq 18 are as follows: $R^2 = 0.9647$, $\alpha = 1.60$ min^{-1}, $-\beta = 4.3 \times 10^{-3}$ min^{-2}.

As in Cases A and C, eq 18 was found to provide the best curve fits to the empirical data in Figure 4A and Figure 4B. That means the conversion is deceleratory (that behavior can also be inferred from the shapes of the transients in the two plots). As mentioned earlier, deceleratory dispersive kinetics are typically linked to denucleation rate-limited phenomena, such as some dissolution events and thermal decompositions of crystals. Thus, an alternate explanation for the observation in which the transformation of BH to A is faster at slower antisolvent addition rates is simply that the rate-limiting step of the conversion is the dissolution of BH (and not the nucleation-and-growth of A).

E. Dissolution of Theophylline Anhydrate: A Case of Dispersive Dissolution Accompanied by a Phase Transformation. In the fifth and final example,[34] Raman spectroscopy was used for in situ monitoring of the solid theophylline (TP) anhydrate as it transformed to the TP monohydrate during the dissolution of a 1:1 (w/w) compact of TP anhydrate and the water-absorbing excipient, MCC. The original workers[34] used the half-life of the transformation as an indicator of the kinetics, but the author believes that a lot of important information is lost in doing that.[35] Regardless, the data presented in Figure 5 for this phase transformation were best able to be fit by eq 18. Once again, that finding supports the (dispersive) dissolution of the anhydrate being the rate-limiting step in the conversion. However, the main reason that this data set was selected is because of the relatively poor fit of the model to the empirical data; that observation is worth some additional discussion.

A general limitation in kinetic modeling exemplified by the transient in Figure 5, is that the random scatter (noise) in the data can significantly diminish the quality of the information that can be extracted from it, even with the best of models. A common limitation of the dispersive kinetic models presented herein, including eq 18, is that they cannot describe "negative conversion data" (either x or p) and they also cannot relate those values that exceed unity (i.e., 100% conversion). That is actually a good thing, as such values are nonphysical. Those are two final points of which workers should be aware when collecting and fitting kinetic data.

Conclusions

The present work put into context the development of the author's models with respect to other important, historically

relevant and more recent, nucleation-and-growth kinetic models. The physicochemical interpretation of the two fit parameters, α and β, used in these dispersive models was described. The mathematics has been verified for accuracy and all assumptions have been noted and justified. Finally, the derivations of the dispersive model equations have been laid out in a systematic and logical manner for ease of understanding.

Given the usefulness and robustness of these dispersive kinetic equations (in precisely fitting a wide assortment of empirical solid-state data pulled from the recent literature), coupled with the physicochemical insights (which can often be gained through the activation parameters) provided via the fit constants, α and β, the continued use of the isothermal models was supported. For completeness, some potential pitfalls encountered in the kinetic modeling with these equations were also addressed, but none detract from their overall usefulness.

Acknowledgment. The author thanks Dr. George X. Zhou of Merck & Co., Inc., for providing him with the data shown in Figure 1 of this work.

References and Notes

(1) Johnson, W. A.; Mehl, R. F. *Trans. AIME* **1939**, *135*, 416.
(2) Avrami, M. *J. Chem. Phys.* **1939**, *7*, 1103.
(3) Avrami, M. *J. Chem. Phys.* **1940**, *8*, 212.
(4) Avrami, M. *J. Chem. Phys.* **1941**, *9*, 177.
(5) Erofe'ev, B. V. *Dokl. Akad. Nauk SSSR* **1946**, *52*, 511.
(6) Prout, E. G.; Tompkins, F. C. *Trans. Faraday Soc.* **1944**, *40*, 488.
(7) Prout, E. G.; Tompkins, F. C. *Trans. Faraday Soc.* **1946**, *44*, 468.
(8) Burnham, A. K.; Braun, R. L. *Energy Fuels* **1999**, *13*, 1.
(9) Khawam, A.; Flannagan, D. R. *J. Phys. Chem. B* **2006**, *110*, 17315.
(10) Khawam, A.; Flanagan, D. R *J. Pharm. Sci.* **2006**, *95*, 472.
(11) Bajzer, Z.; Vuk-Pavloviæc, S. *J. Theoret. Med.* **2000**, *2*, 307.
(12) Demetrius, L. *J. Theor. Biol.* **2006**, *243*, 455.
(13) Plonka, A. *Sci. Rev.* **2000**, *25*, 109.
(14) Plonka, A. *Annu. Rep. Prog. Chem. Sect. C* **2001**, *97*, 91.
(15) Plonka, A. *Annu. Rep. Prog. Chem. Sect. C* **1988**, *85*, 47.
(16) Saen-oon, S.; Quaytman-Machleder, S.; Schramm, V.L.; Schwartz, S. D. *Proc. Natl. Acad. Sci.* **2008**, *105*, 16543.
(17) Skrdla, P. J. *J Phys. Chem. A* **2007**, *111*, 4248.
(18) Skrdla, P. J. *Chem. Phys. Lett.* **2006**, *419*, 130.
(19) Skrdla, P. J. *J. Phys. Chem. A* **2007**, *111*, 11809.
(20) Galwey, A. K. *J. Therm. Anal. Cal.* **2008**, *92*, 967.
(21) Lakshminarayanan, E. S.; Pitchaimani, M. *Appl. Math. Lett.* **2004**, *17*, 173.
(22) Skrdla, P. J. *J. Phys. Chem. A* **2006**, *110*, 11494.
(23) Cheng, Y. C.; Fleming, G. R. *J. Phys. Chem. A* **2008**, *112*, 4254.
(24) See Supporting Information provided with ref 22 available at http://pubs.acs.org.
(25) Skrdla, P. J.; Robertson, R. T. *Thermochim. Acta* **2007**, *453*, 14.
(26) Skrdla, P. J.; Robertson, R. T. *J. Phys. Chem. B* **2005**, *109*, 10611.
(27) Skrdla, P. J. *Cryst. Growth Des.* **2008**, *8*, 4185.
(28) Skrdla, P. J. *J. Pharm. Sci.* **2007**, *96*, 2107.
(29) Skrdla, P. J. *J. Pharm. Biomed. Anal.* **2007**, *45*, 251.
(30) Starbuck, C.; Spartalis, A.; Wai, L.; Wang, J.; Fernandez, P.; Lindemann, C. M.; Zhou, G. X.; Ge, Z. *Cryst. Growth Des.* **2002**, *2*, 515.
(31) Schöll, J.; Bonalumi, D.; Vicum, L.; Mazzotti, M. *Cryst. Growth Des.* **2006**, *6*, 881.
(32) Li, H.; Stowell, J. G.; He, X.; Morris, K. R.; Byrn, S. R. *J. Pharm. Sci.* **2007**, *96*, 1079.
(33) Kitamura, M.; Hironaka, S. *Cryst. Growth Des.* **2006**, *6*, 1214.
(34) Aaltonen, J.; Heinänen, P.; Peltonen, L.; Kortejärvi,Tanninen, V. P.; Christiansen, L.; Hirvonen, J.; Yliruusi, J.; Rantanen, J. *J. Pharm. Sci.* **2006**, *95*, 2730.
(35) Skrdla, P. J. *Biophys. Chem.* **2005**, *118*, 22.

JP904505W